REVIEW

Check for updates

Circularly polarized luminescence of macromolecular co-assembly systems

Ming-Jun Ji,[ab] Meng Li*[ab] and Chuan-Feng Chen [ID] *[ab]

In recent years, materials with circularly polarized luminescence (CPL) properties have attracted increasing attention from both academia and industry due to their promising applications in 3D displays, anti-counterfeiting encryption, optical data storage, bioimaging, and spintronic devices. Among these materials, macromolecular co-assembly systems have emerged as one of the most appealing candidates, offering advantages such as improved processability and enhanced luminescence dissymmetry factors. In this review, we systematically summarize recent representative advances in macromolecular co-assembly systems with CPL properties, categorizing them into three main types: (1) co-assembly systems comprising a macromolecular dye, (2) co-assembly systems comprising a macromolecular chiral inducer, and (3) co-assembly systems comprising both a macromolecular chiral inducer and a macromolecular dye. These systems encompass a wide range of macromolecular structures, including both biomacromolecules and synthetic polymers. Furthermore, we discuss the existing challenges in macromolecular CPL co-assemblies and provide an outlook on future research directions. We believe this review will enable researchers across multiple disciplines to quickly grasp the current status of macromolecular CPL co-assembly systems and inspire further exploration and innovation in this rapidly evolving field.

1. Introduction

Circularly polarized light (CP light) refers to light in which the electromagnetic vector propagates in a circular motion. When it is observed in the direction of propagation, if the electromagnetic vector rotates in a clockwise direction, the light is termed right-handed CP light, and if it rotates counterclockwise, it is termed left-handed CP light (Fig. 1a).[1–3] One of the key parameters of CP light is the luminescence dissymmetry factor (g_{lum}). Depending on the emission mechanism, this dissymmetry factor can be further divided into photoluminescence dissymmetry factor (g_{PL}) and electroluminescence dissymmetry factor (g_{EL}). The g_{lum} value is defined as $g_{lum} = 2(I_L - I_R)/(I_L + I_R)$, where I_L represents the emission intensity of left-handed CP light and I_R represents the emission intensity of right-handed CP light.[4]

[a]Beijing National Laboratory for Molecular Sciences, CAS Key Laboratory of Molecular Recognition and Function, Institute of Chemistry, Chinese Academy of Sciences, Beijing 100190, China. E-mail: cchen@iccas.ac.cn; limeng@iccas.ac.cn

[b]University of Chinese Academy of Sciences, Beijing 100049, China

Ming-Jun Ji received his BS degree from Qufu Normal University in 2021 and MS degree from University of Science and Technology of China in 2024. He then joined the group of Prof. Chuan-Feng Chen as a PhD student at the Institute of Chemistry, Chinese Academy of Sciences. His research interest is in the construction of high-performance circularly polarized luminescent systems and the coordination polymerization of olefins.

Ming-Jun Ji

Meng Li received his PhD from the Institute of Chemistry, Chinese Academy of Sciences in 2015 under the supervision of Prof. Chuan-Feng Chen. He is currently working as an associate professor at Institute of Chemistry, Chinese Academy of Sciences. His research interests focus on chiral optoelectronic materials and devices.
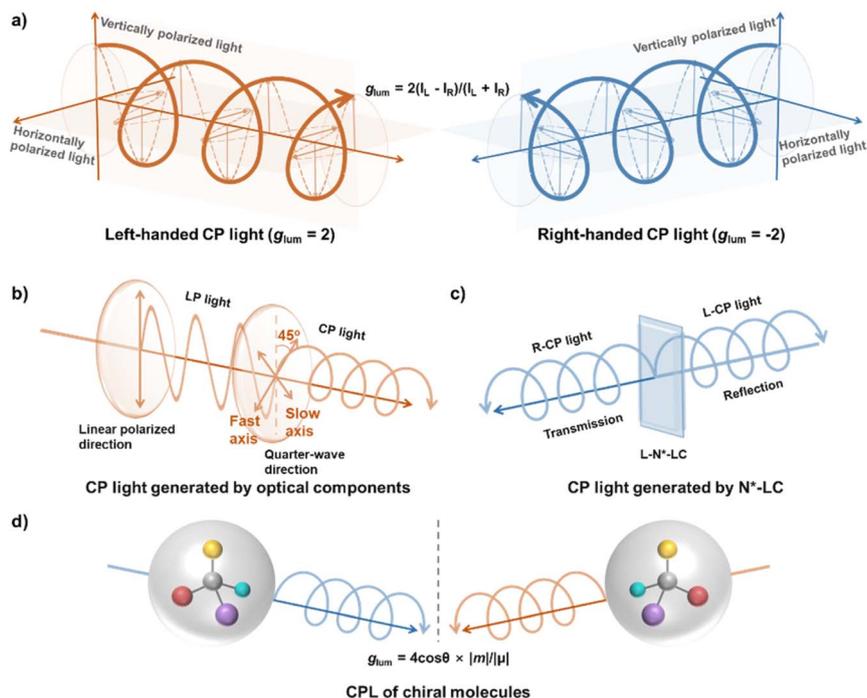
Meng Li

Fig. 1 (a) Schematic illustration of left- and right-handed circularly polarized light and the definition equation of g_{lum}. (b) Diagram showing the generation of circularly polarized light by passing unpolarized light through a linear polarizer and a quarter-wave plate. (c) Schematic representation of the conversion of unpolarized light into circularly polarized light *via* the selective reflection–transmission mechanism of liquid crystals. (d) Illustration of circularly polarized light generation from chiral luminescent molecules under optical excitation, along with the relationship between the g_{lum} value, electric transition dipole moments (μ) and magnetic transition dipole moments (m).

According to this definition, if the light is purely left-handed CP light, the g_{lum} value is +2; for purely right-handed CP light, the g_{lum} value is −2. In cases where the light is unpolarized, linearly polarized, or the emission intensities of left- and right-handed CP light are equal, the g_{lum} value is 0.

Currently, there are several methods to generate CP light. One approach involves optical components, primarily a polarizer and a $\lambda/4$ wave plate (Fig. 1b).[5–7] The polarizer transforms unpolarized light into linearly polarized light (LP light). When this linearly polarized light passes through the $\lambda/4$ wave plate, the resulting light depends on the angle between the linear polarization direction and the fast or slow axis of the wave

Chuan-Feng Chen has been working as a full professor of organic chemistry at Institute of Chemistry, Chinese Academy of Sciences, since 2001. His current research includes supramolecular chemistry based on synthetic macrocyclic hosts, molecular machines and stimulus responsive supramolecular materials, optoelectronic materials and devices, and helicene chemistry.

Chuan-Feng Chen

plate. When the angle between the polarization direction of the linearly polarized light and the fast–slow axis of the wave plate is 45°, the magnitudes of the components along the fast and slow axes are equal, resulting in CP light. For other angles, elliptical polarization is generated. Therefore, by adjusting the angle between the polarizer and the $\lambda/4$ wave plate, it is straightforward to generate pure left-handed or right-handed CP light with a g_{lum} value of ± 2.

Another method to generate CP light with high g_{lum} values is through chiral nematic liquid crystals (N*-LCs), also called cholesteric liquid crystals (CLCs). The mechanism behind high g_{lum} values in chiral nematic liquid crystals is the selective reflection of light by the liquid crystal structure (Fig. 1c).[8–17] The reflection wavelength of N*-LCs follows the Bragg reflection formula: $n\lambda = 2p \times \sin\theta$, where λ is the reflection wavelength, p is the pitch, and θ is the angle between the incident light and the liquid crystal surface. When unpolarized light with a wavelength matching the reflection wavelength of the N*-LC strikes the surface of N*-LC, the light is decomposed into left- and right-handed CP light. Light with the same handedness as the helical twist of the liquid crystal is selectively reflected, while light with the opposite handedness is transmitted. These systems can easily produce CP light with a g_{lum} greater than 1.5. However, in the case of optical components or chiral nematic liquid crystals, generating CP light essentially eliminates one component of the polarization direction in the original unpolarized light, leading to a pure CP light of the opposite handedness. Therefore, both the optical component method (using

polarizers and $\lambda/4$ wave plates) and the selective reflection mechanism of chiral nematic liquid crystals result in significant energy loss, typically greater than 50%.

To overcome the energy loss, researchers have focused on the development of materials with circularly polarized luminescence (CPL) properties (Fig. 1d). Due to their CPL properties, these materials have gained considerable attention for potential applications in fields such as 3D displays, anti-counterfeiting, high-definition displays, and optoelectronic devices.[18–24] However, despite their broad potential, practical applications of CPL materials remain limited. One of the most challenges is the relatively low g_{lum} values, which, in early studies, were only on the order of 10^{-4} to 10^{-3}.[25–29] Therefore, developing new strategies to improve the g_{lum} values is crucial for advancing real applications of CPL materials. The g_{lum} value is related to the electric and magnetic transition dipoles of the system, expressed by the formula $g_{lum} = 4 \cos\theta |\mu||m|/(|\mu|^2 + |m|^2)$, where μ represents the electric transition dipole, m represents the magnetic transition dipole, and θ is the angle between these two dipoles. In most cases, the electric transition dipole is much larger than the magnetic transition dipole ($\mu \gg m$), so the formula can be approximated as $g_{lum} = 4 \cos\theta |m|/|\mu|$. From this, it is clear that the g_{lum} value is proportional to the magnetic transition dipole and inversely proportional to the electric transition dipole. In this case, lanthanide metal complexes can achieve high g_{lum} values, exceeding 1 or even higher.[30–32] This is due to their strong spin–orbit coupling, which enhances the magnetic transition dipole moment. However, in pure organic systems, the high electric transition dipole moment and the negligible magnetic transition dipole moment make achieving a high g_{lum} value a significant challenge.[33,34]

To enhance the g_{lum} values in pure organic systems, a promising strategy is the assembly of chiral molecules. Chiral helical molecular assemblies exhibit strong orbital angular momentum, which can induce spin polarization and spin selectivity through spin–orbit coupling, thereby facilitating an increase in the g_{lum} value.[35–39] These efforts have led to a substantial increase in g_{lum} values of pure organic systems from the 10^{-4} range to the 10^{-2} range.[40–42] Some reviews have summarized these advancements in self-assembled systems.[1,43–45] However, a major challenge in the synthesis of chiral luminescent molecules is the complexity and high cost associated with chiral resolution. To avoid the use of chiral luminescent molecules, recent research studies have shifted toward co-assembly systems formed by achiral dye and chiral inducers, like achiral luminescent small molecules and chiral small molecular inducers.[34,36–51] Except small molecules, macromolecules can also be utilized not only as achiral luminescent materials but also as chiral inducers. Upon chiral co-assembly, these macromolecules exhibit remarkable CPL performance. Furthermore, compared to small molecules, polymers offer greater structural and functional diversity, which can be easily achieved by various synthetic strategies such as homopolymerization, alternating copolymerization, non-strictly alternating copolymerization, random copolymerization, block copolymerization, and homopolymerization. Additionally, polymers possess the advantage of facile processability, making them highly suitable for
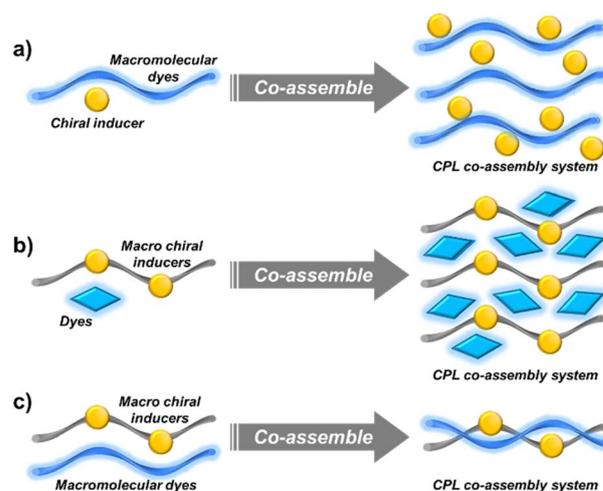

Fig. 2 Classification of macromolecular CPL co-assembly systems as discussed in this review. (a) Co-assembly systems comprising a macromolecular dye. (b) Co-assembly systems comprising a macromolecular chiral inducer. (c) Co-assembly systems comprising both a macromolecular chiral inducer and a macromolecular dye.

practical applications. However, there is currently no comprehensive review that summarizes the work on macromolecular co-assembly systems with CPL, including CPPL and CPEL, properties. Therefore, this review aims to summarize the macromolecular co-assembly systems that can achieve CPL, discussing how factors such as the type of luminescent molecules, chiral dopants, doping ratios, film thickness, and annealing temperatures influence the g_{lum} values of the co-assembly systems. During our review, we found that these co-assembled systems involve not only synthetic polymers but also biomacromolecules such as peptides, deoxyribonucleic acid (DNA), and cellulose. Thus, it should be noted that throughout this article, we predominantly use the term macromolecule rather than polymer. This distinction is made because, in a strict sense, the term macromolecule encompasses both biomacromolecules and synthetic polymers, whereas the term polymer specifically refers to synthetic macromolecules composed of repeating monomeric units.

This review categorizes the discussed CPL co-assembled systems into three types: (1) co-assembly systems comprising a macromolecular dye (Fig. 2a), (2) co-assembly systems comprising a macromolecular chiral inducer (Fig. 2b), and (3) co-assembly systems comprising both a macromolecular chiral inducer and a macromolecular dye (Fig. 2c). We hope this review will provide guidance for the future design of CPL macromolecular co-assembly systems. Additionally, this review focuses specifically on co-assembly systems that directly emit CP light, including photoluminescent and electroluminescent systems, rather than liquid crystal co-assembly systems based on selective reflection.

2. Co-assembly systems from macromolecular dyes

2.1. Binary co-assembly systems

Although CPL co-assembled macromolecular systems have only recently emerged as a research hotspot, several representative

studies were conducted between 2010 and 2020. In 2012, Akagi's group reported a co-assembled macromolecular system using a poly(*para*-phenylene) (PPP, Fig. 3) derivative with terminal quaternary ammonium cation substituents and an axially chiral biphenyl derivative (*R/S*-BNP, Fig. 3) functionalized with long-chain alkoxy sulfonate anions.[52] The introduction of quaternary ammonium cations and sulfonate anions imparted water solubility to PPP and *R/S*-BNP. By dissolving PPP and *R/S*-BNP separately in methanol and water at equal concentrations and mixing them in different volume ratios, a series of PPP–BNP co-assembly systems were formed. These assemblies adopted an intermolecular helical π-stacked structure, stabilized by electrostatic and π–π interactions. The assembled PPP–BNP exhibited CPL activity with a $|g_{lum}|$ value of up to 3.0×10^{-2} in solution. Upon further aggregation, the system formed spherulites (semi-crystalline nanospheres) displaying blue CPL. This was the first example of helically structured spherulites constructed from π-conjugated polymers. This work represents an early milestone in CPL co-assembled macromolecular systems. However, due to aggregation-caused quenching (ACQ), the luminescence intensity of the PPP–BNP assembly was lower than that of PPP alone.

Poly(*p*-phenylene) polymers can generate macromolecular co-assembly systems with CPL properties by chiral co-assembly; however, the most commonly used and more effective polymers in CPL co-assemblies are polyfluorene derivatives, particularly those based on poly[9,9-dioctylfluorene-*co*-benzothiadiazole] (F8BT, Fig. 3). In 2013 and 2017, Fuchter's group[53] and Kim's group[54] employed chiral inducers aza[6]helicene, [7]helicene, and *R/S*-5011 (Fig. 3) to achieve chiral co-assembly with F8BT, respectively. The macromolecular co-assembly systems with CPL properties can successfully integrate into circularly polarized organic light-emitting diodes (CP-OLEDs). While these two

studies seemingly differed only in the choice of chiral inducers, the distinct inducers led to different mechanisms of CP light generation within the co-assemblies. In Fuchter's study, the g_{lum} value of the CPL emission exhibited a strong positive correlation with the helicene doping concentration, while it remained independent of the film thickness. Specifically, when the helicene doping ratio was 7%, g_{PL} and g_{EL} were both 0.2, and at 53% doping g_{PL} and g_{EL} could reach 0.5. This result indicated that the CPL in this macromolecular co-assembly system originated from the chiral dopant itself, meaning that the helicene imposed a helical molecular conformation onto the F8BT host material. In contrast, Kim's study demonstrated that the CPL activity of the 5011–F8BT co-assembled system was strongly dependent on film thickness, with g_{lum} increasing as the thickness increased. At a thickness of 200 nm, $|g_{PL}|$ and $|g_{EL}|$ of the co-assembly system reached remarkably high values of 0.72 and 1.13, respectively. Additionally, a uniform twisted alignment was achieved only after thermal annealing, which is essential for the generation of CPL properties. These findings suggest that *R/S*-5011, possessing a high helical twisting power (HTP), induced macroscopic twisted stacking of the F8BT host in this co-assembly system, differing from the direct molecular-scale helical conformation formation observed in Fuchter's system. Moreover, the exceptionally high g_{lum} values achieved in Kim's work were not solely due to the high HTP of 5011. His study also incorporated a polyimide (PI) friction-aligned layer, which facilitated a more ordered co-assembly of 5011 and F8BT, further enhancing the g_{lum}. If without friction alignment, the co-assembled film exhibited CPL with only $|g_{PL}| = 0.46$ and $|g_{EL}| = 0.71$. The pioneering contributions of Fuchter and Kim provided valuable insights for the future design of CPL co-assembled macromolecular systems, particularly for circularly polarized electroluminescent (CPEL) devices.

Entering the 2020s, macromolecular-based CPL co-assembled systems have yielded numerous significant advancements, with notable contributions from research groups such as Cheng, Chen, and Zhang. Over the past five years, these studies have greatly expanded the understanding of CPL macromolecular co-assembly systems. Early work by Cheng's group demonstrated that linking the two oxygen atoms of axially chiral binaphthol *via* a methylene bridge resulted in binaphthol derivatives with a locked dihedral angle, thereby enhancing molecular rigidity and improving chiral induction ability.[55,56] On the other hand, pyrene and its derivatives are essential blue-emitting chromophores with strong supramolecular assembly capabilities.[57–60] Thus, Cheng's research focused on using binaphthol derivatives with a locked dihedral angle (*R/S*-M, Fig. 4) as chiral inducers, while pyrene-containing polymers served as luminescent polymers to construct CPL co-assembled systems with various properties. In 2022, they utilized chiral inducers *R/S*-M with a locked dihedral angle to co-assemble with polymers containing liquid crystalline segments (LC-P1, LC-P2, and LC-P3, Fig. 4).[61] Through optimization of the doping ratio, they found that at a 10% doping level of *R/S*-M, the resulting $(R/S\text{-M})_{0.1}$–$(P)_{0.9}$ exhibited the most efficient chiral assembly. The corresponding g_{PL} values of the co-assembled LC-P1, LC-P2, and LC-P3 systems reached 2.23 ×
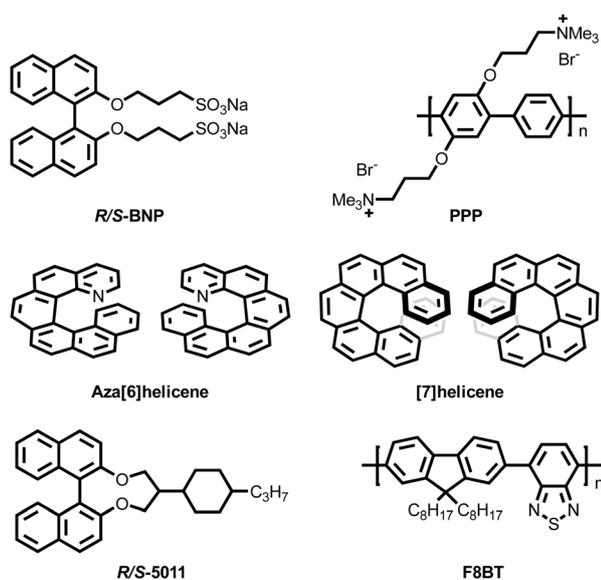

Fig. 3 Chiral inducers and luminescent macromolecules used for constructing binary co-assembly systems with CPL properties generated by Akagi's group, Fuchter's group and Kim's group.
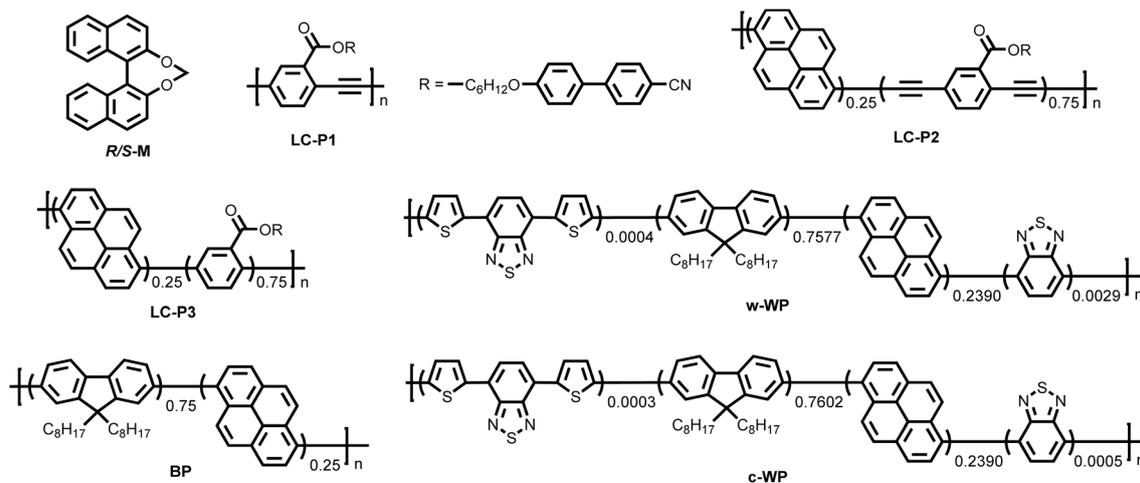
Fig. 4 Chiral inducers and luminescent macromolecules used for constructing binary co-assembly systems with CPL properties based on R/S-M generated by Cheng's group.

10^{-2}, 2.25×10^{-2}, and 6.47×10^{-2}, respectively. The higher g_{PL} value of LC-P3 compared to LC-P1 and LC-P2 was attributed to the relatively flexible polymer backbone of LC-P3. Furthermore, this flexibility facilitated helical nanofiber configuration inversion upon thermal annealing, leading to a reversal of the CPL signal. For instance, $(S\text{-M})_{0.1}$–$(\text{P3})_{0.9}$ exhibited a negative CPL signal below 95 °C (determined solely by the chiral inducer S-M), but upon annealing above 100 °C, the signal reversed to positive. This work developed a strategy by using thermal annealing of macromolecular-based chiral co-assembly materials to achieve direction adjustable CPL.

In recent years, white circularly polarized luminescence (WCPL) has attracted increasing attention from both academia and industry due to its potential applications in next-generation lighting and flat-panel displays.[62,63] In 2023, Cheng and colleagues synthesized three achiral conjugated random copolymers, BP, c-WP, and w-WP (Fig. 4), by copolymerizing the blue-emitting 9,9-dioctylfluorene (FO), the green-emitting 2,1,3-benzothiadiazole (BT), and the red-emitting 4,7-di(thiophen-2-yl)benzo[c][1,2,5]thiadiazole (DTBT).[64] By tuning the composition of copolymers, they obtained blue (BP), cool white (c-WP), and warm white (w-WP) emitting copolymers with the Commission Internationale de l'Éclairage (CIE) coordinates of (0.18, 0.21), (0.44, 0.44), and (0.33, 0.36), respectively. Subsequently, these three copolymers were co-assembled with the locked dihedral angle chiral inducer R/S-M. Due to π–π stacking interactions and the formation of well-ordered helical nanofibers, the resulting co-assembled systems exhibited CPL activity. Optimization of the doping ratio revealed that the most efficient chiral assembly was achieved at a 20% R/S-M content, leading to the highest g_{lum} values. $(R/S\text{-M})_{0.2}$–$(\text{BP})_{0.8}$ exhibited $|g_{PL}| = 4.3 \times 10^{-2}$ at 438 nm, while $(R/S\text{-M})_{0.2}$–$(\text{w-CP})_{0.8}$ and $(R/S\text{-M})_{0.2}$–$(\text{c-WP})_{0.8}$ reached $|g_{PL}|$ values of 3.6×10^{-2} and 5.3×10^{-2}, respectively. More importantly, when integrated into devices, $(R/S\text{-M})_{0.2}$–$(\text{c-WP})_{0.8}$ as the emissive layer (EML) demonstrated outstanding white circularly polarized electroluminescence performance, with CIE coordinates of (0.33, 0.33),

a remarkably high color rendering index (CRI) exceeding 80 and reaching 98, and an impressive $|g_{EL}|$ of 8.7×10^{-2}. These results represented the highest performance level of CP-WOLEDs at that time and provided a viable strategy for high-performance CP-WOLED design.

Chen's research group has focused on utilizing the highly helically twisted chiral inducer R/S-5011 to construct CPL co-assembled systems with diverse properties. In 2024, they synthesized a novel chiral polymer (R/S-PBN, Fig. 5a) by linking axially chiral binaphthyl to a boron–nitrogen (BN) unit and copolymerizing it with 9,9-dihexylfluorene.[65] This polymer exhibited excellent self-assembly properties. The resulting self-assembled system demonstrated narrowband CPL emission with a full-width at half-maximum (FWHM) of 29 nm, a photoluminescence quantum yield (PLQY) of 79%, and a $|g_{PL}|$ value reaching 0.11. When incorporated as the EML in a device, the system achieved a CPL electroluminescence (CPEL) with an FWHM of 36 nm, an external quantum efficiency (EQE) of 9.8%, and a $|g_{EL}|$ of 0.07. This work represented the first example of a self-assembled chiral polymer simultaneously achieving high EQE, large g_{EL}, and narrowband emission.

Stimuli-responsive CPL materials have garnered significant attention for their applications in optical information storage and encryption.[66] In the same year, Chen's group developed a novel non-chiral conjugated polymer, PFIQ (Fig. 5b), by copolymerizing isoquinoline with 9,9-dioctylfluorene.[67] By co-assembling PFIQ with R/S-5011 at a 7:3 ratio, they obtained a pair of CPL co-assemblies, P7R3 and P7S3, which exhibited a remarkable $|g_{PL}|$ value of 0.3. Notably, the isoquinoline units in PFIQ enabled reversible protonation and deprotonation, allowing for reversible tuning of the emission color via simple acid/base vapor treatment. This reversible acid–base response provided an effective strategy for information encryption and decryption. More importantly, this co-assembled system successfully realized CPL energy transfer (CPL-ET), wherein the CPL generated by P7R3 and P7S3 effectively excited multicolor non-chiral emitters to produce secondary CPL emission. This
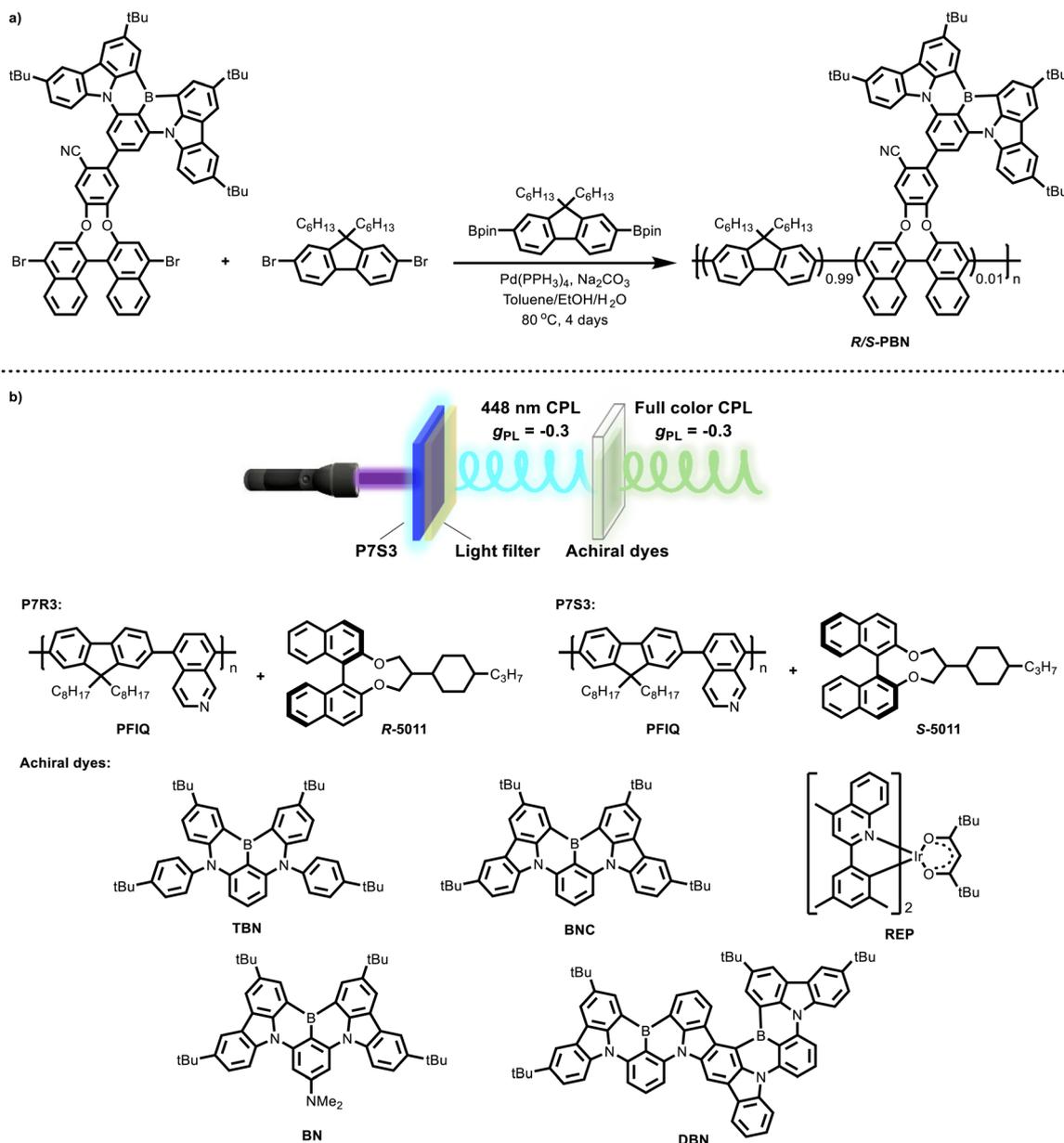
Fig. 5 (a) Structure of R/S-PBN prepared by Chen's group. (b) The schematic representation of the CPL energy transfer process and the structures of the PFIQ, R/S-5011 and achiral luminescent small molecules used by them.

study marked the first demonstration of a CPL system where the emitted CP light from non-chiral molecules retained the same g_{lum} value as the incident CP light (Fig. 5b). Leveraging the reversible acid–base response of P7R3 and P7S3 along with the CPL-ET mechanism, the system was further applied in the construction of multi-level logic gates, showcasing its potential for advanced optical information processing.

Beyond the contributions from Cheng' research group and Chen's research group, there have been additional advancements in the co-assembly of chiral inducers and macromolecular dyes for constructing CPL co-assembled systems. From the perspective of WCPL, achieving precise and dynamic control of CPL in co-assembly films remains a significant challenge.

Zhang's group also worked on macromolecule-based CPL systems.[68–75] In 2024, Zhang's group introduced an addition-subtraction principle for polymer systems. Unlike Cheng's approach, which directly synthesized white-light-emitting polymers through copolymerization of red, green, and blue (RGB) monomers (Fig. 6a), Zhang's strategy involved blending three polyfluorene-based copolymers (P1, P2, and P3, each emitting in the blue, green, and red spectral regions, respectively), to achieve white-light emission in polymer assemblies (Fig. 6b).[76] By systematically tuning the doping ratio of these polymers and correlating the resulting co-assembly systems with the CIE coordinates, they established a linear relationship: $CIE(x, y) = f(P1, P2, P3)$. Building upon this principle, a co-
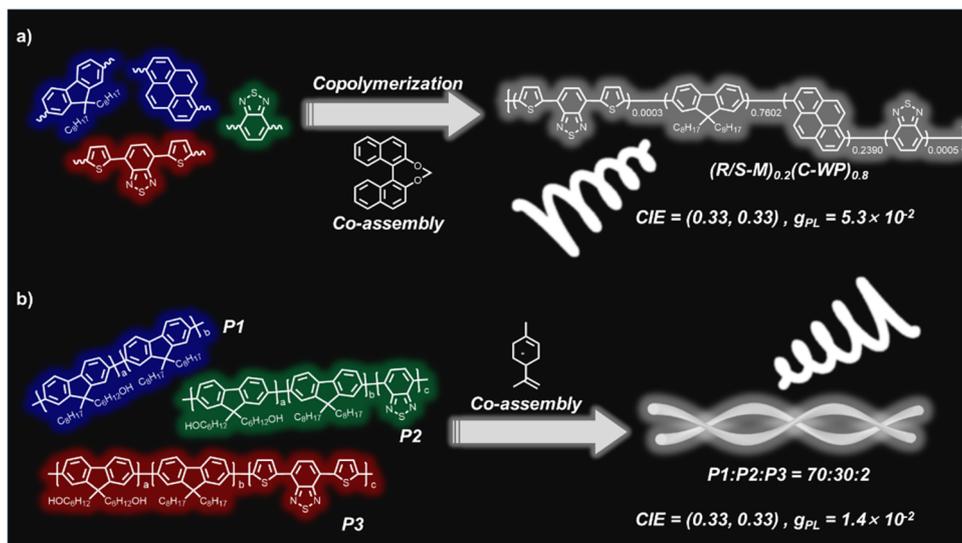
Fig. 6 (a) Schematic strategy of Cheng's group for constructing a white CPL co-assembly system. (b) Schematic strategy of Zhang's group for constructing a white CPL co-assembly system.

assembled film with an ideal white CPL emission (CIE coordinates = (0.33, 0.33), $|g_{PL}| = 1.4 \times 10^{-2}$, and PLQY = 80.8%) was obtained when P1, P2, and P3 were blended at a 70 : 30 : 2 ratio and assembled *via* evaporation onto a quartz substrate induced by chiral limonene. Furthermore, after removing the chiral source (limonene) and performing an acetal reaction to crosslink the polymers, the resulting crosslinked film retained its CPL properties, demonstrating the structural stability of the chiral co-assembly (Table 1).

Regarding the types of chiral inducers, the aforementioned studies primarily employed axial chiral inducers, central chiral limonene, and helically chiral spirocyclic inducers. In 2024, Mazaki's group developed and utilized CPL-active planar chiral carbazole-substituted [2.2]paracyclophane ([2.2]PC) derivatives, R/S-1a (Fig. 7, $|g_{PL}|$ up to 4.7×10^{-4}) and R/S-1b ($|g_{PL}|$ up to 3.2×10^{-4}), as chiral inducers.[77] These molecules co-assembled with F8BT *via* π–π interactions to form the 1a–F8BT and 1b–F8BT assemblies. When the chiral dopant concentration was set at

3%, R/S-1a–F8BT exhibited a $|g_{PL}|$ value of 1.0×10^{-2} at 548 nm. However, the introduction of bulky *tert*-butyl groups in R/S-1b disrupted π–π interactions between the carbazole moiety and the F8BT backbone, leading to R/S-1b–F8BT to exhibit a lower $|g_{PL}|$ of 2.6×10^{-3} at 548 nm.

2.2. Ternary co-assembly systems

In Section 2.1, we discussed various binary co-assembled systems comprising chiral inducers and emissive polymers. Some of them have even been successfully applied in CP-OLEDs. These pioneering studies have introduced novel chiral inducers and luminescent molecular architectures, as well as innovative assembly strategies for CPEL. However, the relatively low EQE of these binary co-assembled systems has limited the overall performance of CP-OLED devices. Therefore, achieving high $|g_{EL}|$ values while simultaneously enhancing EQE remains a critical challenge for optimizing CP-OLED performance. To

Table 1 CPPL properties of the macromolecular dyes in binary co-assembly systems

| Entry	Assembly systems	PL (nm)	PLQY (%)	$|g_{PL}|$ (10^{-2})	Ref.
1	R/S-BNP–PPP	414	—	3.1	52
2	Aza[6]helicene–F8BT	580	—	50	53
3	[7]Helicene–F8BT	580	—	50	53
4	R/S-5011–F8BT	546		72	54
5	R/S-M–LC-P1	510	6.2	2.23	61
6	R/S-M–LC-P2	565	6.9	2.25	61
7	R/S-M–LC-P3	455	48.5	6.47	61
8	R/S-M–BP	458	38	4.3	64
9	R/S-M–w-WP	452/528/606	41	3.6	64
10	R/S-M–c-WP	456/518/606	42	5.3	64
11	R/S-5011–PFIQ	435	79	30	67
12	R/S-Limonene–P1–P2–P3	464/525/624	80.8	1.4	76
13	R/S-1a–F8BT	548	—	1.0	77
14	R/S-2a–F8BT	548	—	0.26	77
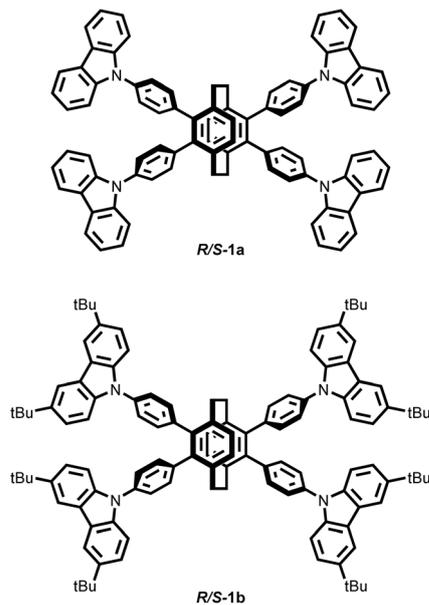
Fig. 7 Chiral inducers and luminescent macromolecules used for constructing binary co-assembly systems with CPL properties generated by Mazaki's group.

address this issue, both Cheng's group and Chen's group employed Förster resonance energy transfer (FRET) processes in 2023 and 2024, respectively, to enhance the EQE of co-assembled CP-OLEDs. In 2023, Cheng's group designed chiral inducers R/S-1Cz and R/S-2Cz (Fig. 8a), which are carbazole-substituted, axially chiral binaphthyl derivatives.[78] These inducers were co-assembled with poly(9,9-dioctylfluorene-co-pyridine) (PFpy, Fig. 8a) as the emissive polymer. At a chiral dopant concentration of 20%, the $(R/S$-2Cz$)_{0.2}$–(PFpy$)_{0.8}$ system

exhibited the most effective chiral assembly, achieving a $|g_{PL}|$ of 3.4×10^{-2} at 454 nm. However, due to random stacking between PFpy and the structurally asymmetric R/S-1Cz, the $(R/S$-1Cz$)_{0.2}$–(PFpy$)_{0.8}$ system showed no significant CPL signal before or after thermal annealing. To further enhance the system's performance, a red phosphorescent iridium complex, Ir(MDQ)$_2$(acac) (Fig. 8a), was introduced at a 10% doping level, forming the ternary co-assembled system $(R/S$-2Cz$)_{0.2}$–(PFpy$)_{0.8}$–(Ir(MDQ)$_2$)$_{0.1}$. The presence of intermolecular FRET and chiral energy transfer resulted in red CPL emission, achieving a $|g_{PL}|$ of 0.02 at 606 nm. Moreover, the PLQY increased to 32.8%, significantly higher than the 20.3% observed in the binary system $(R/S$-2Cz$)_{0.2}$–(PFpy$)_{0.8}$ without Ir(MDQ)$_2$(acac). These findings demonstrated that incorporating emissive small molecules could enhance the overall photoluminescence performance. Encouraged by these results, Cheng's group further employed the ternary co-assembled $(R/S$-2Cz$)_{0.2}$–(PFpy$)_{0.8}$–(Ir(MDQ)$_2$)$_{0.1}$ system as the EML in a CP-OLED device. The resulting device exhibited a $|g_{EL}|$ of 0.014 at 620 nm and, more importantly, achieved an EQE of 4.1%. $|g_{EL}|$ and EQE are the key metrics for CP-OLEDs, so Chen's group introduced the Q-factor concept in 2024 to provide a more intuitive metric for evaluating and comparing the CP-OLED performance.[79] The Q-factor is defined as the product of EQE and $|g_{EL}|$, given by $Q = $ EQE $\times |g_{EL}|$. Applying this formula, the Q-factor of Cheng's CP-OLED, based on $(R/S$-2Cz$)_{0.2}$–(PFpy$)_{0.8}$–(Ir(MDQ)$_2$)$_{0.1}$, was calculated as 5.74×10^{-4} (Table 2).

In the same year, Chen's group developed another high-performance CP-OLED system using the axially chiral R/S-5011 as the chiral inducer and F8BT as the macromolecular dye (Fig. 8b).[80] A binary co-assembled system, (F8BT)$_{0.9}$–(R/S-5011)$_{0.1}$, was first prepared with 10% chiral dopant concentration. To enable an efficient FRET process, a multi-resonance
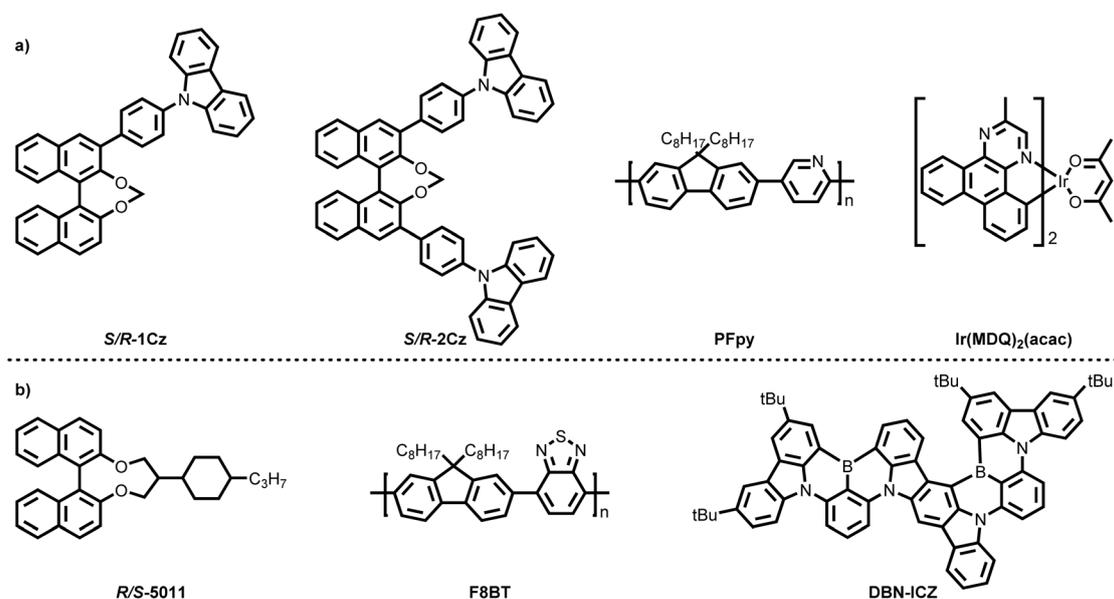

Fig. 8 Chemical structures of chiral inducers, luminescent macromolecules, and achiral luminescent small molecules used by Cheng's group (a) and Chen's group (b) to construct ternary CPL co-assembly systems.

Table 2 CPL properties of the macromolecular dyes in ternary co-assembly systems

Entry	Assembly systems	PL (nm)	PLQY (%)	$\lvert g_{PL} \rvert$	EL (nm)	EQE (%)	g_{EL}	Q-Factor (10^{-3})	Ref.
1	$(R\text{-}2Cz)_{0.2}$–$(PFpy)_{0.8}$–$(Ir(MDQ)_2)_{0.1}$	606	—	0.02	620	3.4	+0.013	0.442	78
2	$(S\text{-}2Cz)_{0.2}$–$(PFpy)_{0.8}$–$(Ir(MDQ)_2)_{0.1}$	606			620	4.1	−0.014	0.574	78
3	$(F8BT)_{0.9}$–$(R\text{-}5011)_{0.1}$–$(DBN\text{-}ICZ)_{0.0005}$	554	79	0.26	552	4.6	+0.16	7.36	80
4	$(F8BT)_{0.9}$–$(S\text{-}5011)_{0.1}$–$(DBN\text{-}ICZ)_{0.0005}$	554			552	4.4	−0.11	4.84	80

thermally activated delayed fluorescence (MR-TADF) emitter, DBN-ICZ (Fig. 8b), was selected as the FRET acceptor due to its absorption band matching the emission spectrum of $(F8BT)_{0.9}$–$(R/S\text{-}5011)_{0.1}$. At a doping concentration of 0.5%, the resulting ternary co-assembled system, $(F8BT)_{0.9}$–$(R/S\text{-}5011)_{0.1}$–$(DBN\text{-}ICZ)_{0.0005}$, achieved complete intermolecular energy transfer. This system exhibited efficient, narrowband CPL emission at 554 nm, with a $\lvert g_{PL} \rvert$ of 0.26, a FWHM of 37 nm, and a PLQY of 79%. When integrated as the EML in a CP-OLED device, the ternary co-assembled system demonstrated outstanding device performance. The resulting CP-OLED exhibited a FWHM of only 39 nm at 552 nm, a $\lvert g_{EL} \rvert$ of 0.16, and an EQE of 4.6%, the highest efficiency reported among chiral co-assembled CP-OLEDs to date. Using the Q-factor formula, the device achieved a record-high Q-factor of 7.36 × 10^{-3}, the highest value among all reported CP-OLEDs to date.

3. Co-assembly systems from macromolecular chiral inducers

3.1. Binary co-assembly systems

Macromolecules can serve not only as emissive components in chiral co-assembled systems but also as macromolecular chiral inducers. In this section, we introduce several representative macromolecular chiral inducers used for chiral assembly, including biomacromolecules such as DNA, polypeptides, and cellulose, as well as synthetic macromolecular chiral inducers, namely chiral polymers. DNA, with its characteristic double-helix structure, is one of the most well-known naturally occurring chiral macromolecules. In the early studies on chiral co-assembly, considerable efforts were dedicated to transferring DNA's chirality to dye molecules to achieve CPL. However, these studies suffered from severe fluorescence quenching due to the ACQ effect of the dyes, leading to compromised CPL performance.[81] In 2019, Ding et al. addressed this issue by employing a carbazole-based cyanine dye (abbreviated as CzCy in this review, Fig. 9) as the emissive dye.[82] The presence of quaternary ammonium cations on CzCy enabled strong electrostatic interactions with the phosphate anions in the DNA backbone, facilitating co-assembly. Importantly, the restriction of intramolecular rotation (RIR) in the assembled CzCy molecules endowed them with aggregation-induced emission (AIE) properties, enhancing the fluorescence of the assembled system.[83] As a result, the DNA–CzCy complex exhibited yellow CPL with a $\lvert g_{PL} \rvert$ of approximately 1.7 × 10^{-3}. Similarly, chiral polypeptides can also function as macromolecular chiral inducers. In 2021, Li et al. developed a de novo-designed chiral amyloid

fibril, T1 ($R_1G_2Y_3F_4W_5A_6G_7D_8Y_9N_{10}Y_{11}F_{12}$, Fig. 9), which was co-assembled with the rotor-type dye thioflavin T (ThT, Fig. 9), a commonly used probe for amyloid fibrils. This chiral co-assembly exhibited a distinct CPL signal with a $\lvert g_{PL} \rvert$ reaching 10^{-2}.[84]

Beyond biomacromolecules, synthetic chiral polymers have also been explored as chiral inducers for CPL co-assembled systems. In 2022, Cheng et al. synthesized two chiral polymeric inducers, R/S-P1 and R/S-P2 (Fig. 9), through the copolymerization of axial chiral monomers with 9,9-dihexylfluorene.[85] The key difference between these two polymers was that R/S-P2 contained an anchored dihedral angle, whereas R/S-P1 did not. These chiral polymers were co-assembled with the achiral dye NPy (Fig. 9) to form two binary chiral assemblies: R/S-P1–NPy and R/S-P2–NPy. At the optimal doping ratio, the assembled systems $(R/S\text{-}P1)_{0.6}$–$(NPy)_{0.4}$ and $(R/S\text{-}P2)_{0.6}$–$(NPy)_{0.4}$ were obtained. Due to the presence of the anchored dihedral angle in R/S-P2, it exhibited a stronger chiral induction effect on NPy, resulting in superior CPL performance. Specifically, $(R/S\text{-}P2)_{0.6}$–$(NPy)_{0.4}$ exhibited a PLQY of 38.8% and a $\lvert g_{PL} \rvert$ of 5.6 × 10^{-2} at 490 nm, significantly outperforming $(R/S\text{-}P1)_{0.6}$–$(NPy)_{0.4}$, which exhibited a PLQY of 25.6% and a $\lvert g_{PL} \rvert$ of 9.2 × 10^{-3} at the same wavelength. Furthermore, when $(R/S\text{-}P2)_{0.6}$–$(NPy)_{0.4}$ was employed as the EML in an OLED device, the resulting device generated a CPEL signal with a $\lvert g_{EL} \rvert$ of 4.8 × 10^{-2} at 489 nm and an EQE of up to 0.21% (Table 3).

3.2. Ternary co-assembly systems

In 2022, Deng's research group developed a ternary co-assembled system comprising racemic helical polyacetylene (racemic P1, Fig. 10), biocompatible chiral polylactic acid (chiral PLA, Fig. 10), and achiral luminescent molecules (NR, X18, and TPE, Fig. 10).[86] Within this co-assembly process, chirality underwent a two-step transfer. The first chirality transfer occurred during the formation of solid cast films, where chiral PLA played a dual role as both the chiral source and the film-forming matrix. Due to the presence of hydrogen bonding as the primary driving force, chirality was successfully transferred from chiral PLA to P1, inducing helical chirality in the initially racemic main chain and resulting in pronounced optical activity. The second chirality transfer involved the subsequent transfer of the induced helical chirality from P1 to the achiral luminescent molecules. As a result, the final co-assembled system exhibited RGB tricolor and white CPL, achieving a maximum $\lvert g_{PL} \rvert$ of 8 × 10^{-3}. This system also demonstrated promising potential for application in CP-OLEDs.
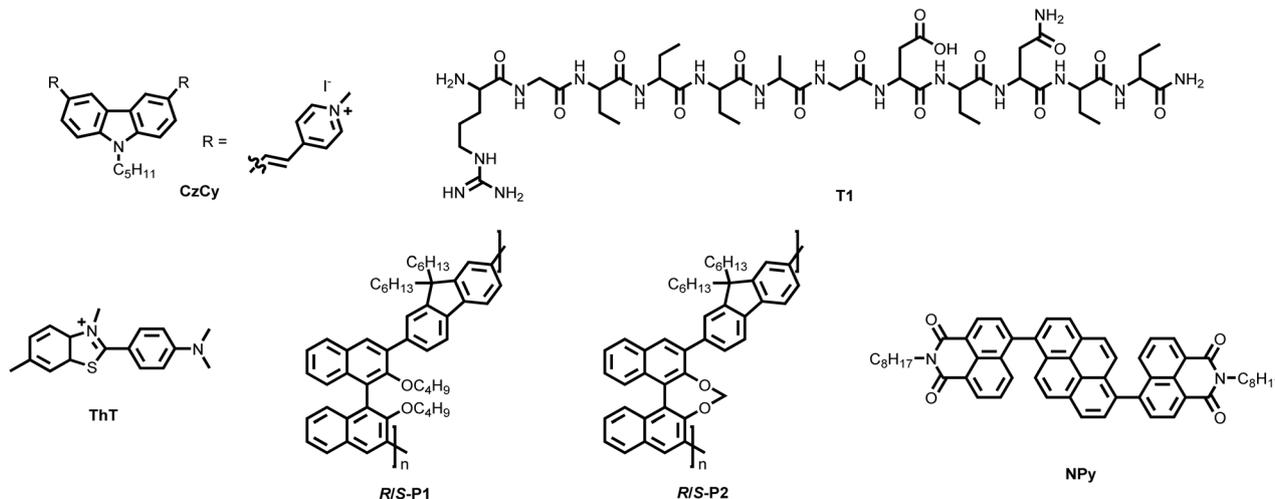
Fig. 9 Chemical structures of macromolecular chiral inducers and achiral luminescent small molecules used to form binary CPL co-assembly systems.

Table 3 CPPL properties of the macromolecular chiral inducers in binary co-assembly systems

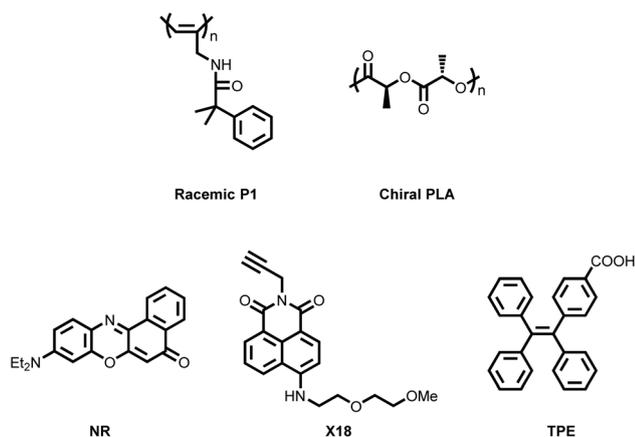| Entry	Assembly systems	PL (nm)	PLQY (%)	$|g_{PL}|$ (10^{-3})	Ref.
1	DNA–CzCy	550	—	1.7	82
2	T1–ThT	488	—	50	84
3	$(R/S\text{-P1})_{0.6}–(\text{NPy})_{0.4}$	490	25.6	9.2	85
4	$(R/S\text{-P2})_{0.6}–(\text{NPy})_{0.4}$	490	38.8	56	85

Fig. 10 Chemical structures of macromolecular chiral inducers, polymer hosts, and achiral luminescent small molecules used to construct ternary CPL co-assembly systems.

Chiral macromolecules and their assembled systems not only served as chiral inducers but have also been recently explored as chiral optical filters that convert unpolarized light into circularly polarized light through selective absorption. For instance, in 2025, Deng's research group reported a co-assembled film with chiroptical properties, prepared from cellulose acetate butyrate (CAB, Fig. 11) and racemic polyacetylene (PM1, Fig. 11).[87] When this CAB–PM1 film was placed

behind the achiral luminescent molecules (CM, ACA, BPEA, and R6G, NR, Fig. 11), one circularly polarized component of the emitted unpolarized light was selectively absorbed by the CAB–PM1 film, resulting in transmitted light with circular polarization. Through this selective absorption mechanism, full-color and white CPL were achieved, with $|g_{PL}|$ values reaching up to 1.5×10^{-2}. Deng's group has also conducted other studies based on the selective absorption properties of chiral polymers; however, they are beyond the scope of this review.[88,89] Moreover, this mechanism is analogous to the selective reflection process
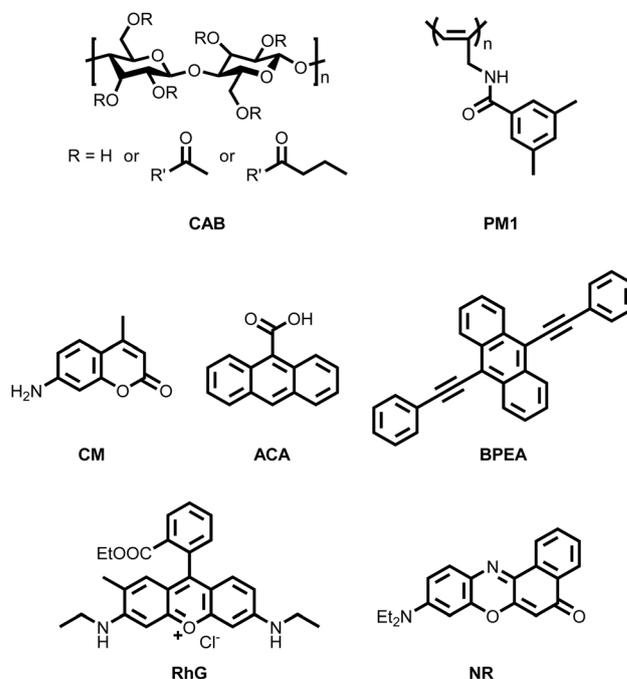

Fig. 11 Chemical structures of macromolecular chiral inducers and polymer hosts used by Deng's group to develop binary co-assembly systems with CD absorption filtering properties.

observed in N*-LC systems mentioned in the Introduction, as both rely on polarization separation. Consequently, they inherently lead to at least 50% energy loss.

4. Co-assembly systems from macromolecular chiral inducers and macromolecular dyes

Macromolecules can serve as chiral macromolecular inducers when co-assembled with luminescent small molecules, or they can function as luminescent macromolecules when co-assembled with chiral small-molecule inducers. In both cases, the resulting co-assembled systems exhibit CPL properties. Similarly, co-assembly between chiral macromolecular inducers and luminescent macromolecules has also been explored, further expanding the design strategies for CPL co-assembly systems. For example, in 2025, Cheng's group synthesized a new class of chiral inducers by copolymerizing the locked dihedral angle chiral inducer with fluorene, yielding the chiral polymer R/S-FO (Fig. 12).[90] Additionally, they copolymerized phenyl (Ph), naphthyl (Na), and pyrenyl (Py) groups at a 25% ratio with 9,9-dioctylfluorene to generate three types of non-chiral conjugated polymers: PFPh, PFNa, and PFPy (Fig. 12). These polymers were then co-assembled with R/S-FO at a 9:1 ratio. Due to π–π stacking interactions, the resulting co-assemblies formed helical nanofibers. The $|g_{PL}|$ values of $(R/S\text{-FO})_{0.1}$–$(\text{PFPh})_{0.9}$, $(R/S\text{-FO})_{0.1}$–$(\text{PFNa})_{0.9}$, and $(R/S\text{-FO})_{0.1}$–$(\text{PFPy})_{0.9}$ reached 1.18×10^{-2}, 2.02×10^{-2}, and 8.53×10^{-3}, respectively. Notably, the highest g_{PL} value was observed in the $(R/S\text{-FO})_{0.1}$–$(\text{PFNa})_{0.9}$ system, likely due to enhanced compatibility between the naphthyl units in PFNa and the binaphthyl segments in R/S-FO. Consistent with the photoluminescence results, when these co-assembled systems were incorporated into devices as EMLs, $(R/S\text{-FO})_{0.1}$–$(\text{PFNa})_{0.9}$ exhibited the highest $|g_{EL}|$ of 1.4×10^{-2}. These

Fig. 12 Chemical structures of macromolecular chiral inducers and luminescent macromolecules used by Cheng's group to construct binary CPL co-assembly systems.

findings underscore the importance of molecular design strategies in optimizing CPL co-assembly systems and pave the way for further advancements in high-performance CP-OLEDs. Although some combinations of chiral macromolecular inducers and luminescent macromolecules have demonstrated good chiral assembly and CPL performance, such systems remain relatively scarce. Further research is needed to expand and refine this approach (Table 4).

5. Application of the CPL co-assembled macromolecular systems in CP-OLEDs

By replacing the EML of conventional organic light-emitting diodes (OLEDs), which typically emit unpolarized light, with a CPL system, OLED devices can be endowed with CPL properties. These devices are known as circularly polarized OLEDs (CP-OLEDs).[2,6] The motivation behind developing CP-OLEDs lies in achieving high $|g_{EL}|$ (approaching 2.0) and circumventing the theoretical 50% energy loss from optical components. In this context, an ideal CP-OLED should simultaneously exhibit a high $|g_{EL}|$ (approaching 2.0), an EQE exceeding 50%, and a Q-factor greater than 1.

Compared to earlier CP-OLEDs based on chiral small organic molecules, those employing macromolecules-based supramolecular assemblies have demonstrated clear advantages, particularly in terms of $|g_{EL}|$ and the overall device performance (Q-factor). Chiral small molecular CP-OLEDs typically showed very low $|g_{EL}|$ values in the range of 10^{-4} to 10^{-3}. In contrast, macromolecule-based CP-OLEDs, as reviewed herein, consistently achieve $|g_{EL}|$ values exceeding 10^{-2}. For instance, systems reported by Cheng's group, such as $(R/S\text{-M})_{0.2}$–$(\text{c-WP})_{0.8}$,[64] $(R/S\text{-2Cz})_{0.2}$–$(\text{PFpy})_{0.8}$–$(\text{Ir(MDQ)}_2)_{0.1}$,[78] $(R/S\text{-P2})_{0.6}$–$(\text{NPy})_{0.4}$,[85] and $(R/S\text{-FO})_{0.1}$–$(\text{PFNa})_{0.9}$,[90] as well as the R/S-PBN systems from Chen's group,[65] have yielded $|g_{EL}|$ values of 8.7×10^{-2}, 1.4×10^{-2}, 4.8×10^{-2}, 1.4×10^{-2}, and 7.0×10^{-2}, respectively. With further tuning, such as employing helicenes or highly twisted R/S-5011 as chiral inducers, adjusting the film thickness, or optimizing thermal annealing conditions, $|g_{EL}|$ values can reach up to the 10^{-1} range. Notably, CP-OLEDs constructed from systems such as aza[6]helicene–F8BT (Fuchter's group),[53] R/S-5011–F8BT (Kim's group),[54] and $(\text{F8BT})_{0.9}$–$(R\text{-5011})_{0.1}$–$(\text{DBN-ICZ})_{0.0005}$ (Chen's group)[80] have achieved $|g_{EL}|$ values as high as 0.5, 0.72, and 0.16, respectively, which is 100 to 1000 times greater than those of chiral-small-molecule-based CP-OLED devices. However, despite their superior $|g_{EL}|$ values, CP-OLEDs based on macromolecular assemblies often suffer from significantly lower EQEs compared to their chiral small-molecule counterparts. The highest EQE reported to date for a macromolecule-based CP-OLED is 4.6%, from the $(\text{F8BT})_{0.9}$–$(R\text{-5011})_{0.1}$–$(\text{DBN-ICZ})_{0.0005}$ system developed by Chen's group.[80] In contrast, chiral small-molecule-based CP-OLEDs have reached EQEs as high as 35.5%, also reported by Chen's group.[79] This suggests that the EQE of chiral small-molecular devices can be nearly an order of magnitude higher than that of macromolecule-based systems. Nevertheless, due to their remarkably high $|g_{EL}|$
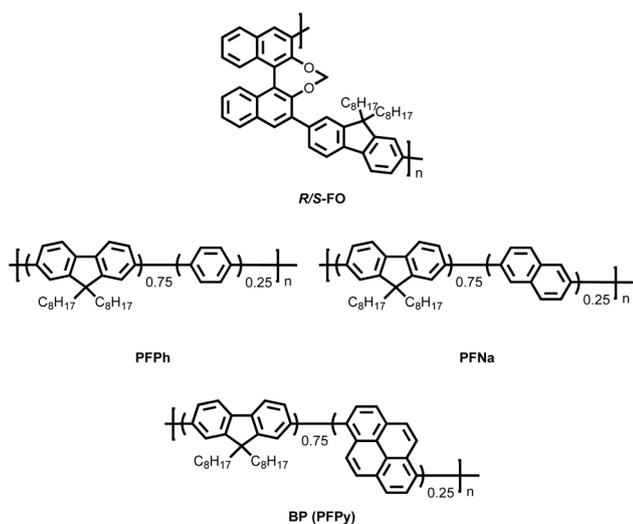
Table 4 CPL properties of the macromolecular chiral inducer and macromolecular dye systems

Entry	Assembly systems	PL (nm)	PLQY (%)	$|g_{PL}| (10^{-2})$	EL (nm)	EQE (%)	$|g_{EL}| (10^{-2})$	Ref.
1	$(R/S\text{-FO})_{0.1}–(PFPh)_{0.9}$	423	11.08	1.13	424	0.64	1.1	90
		444		1.18	448		0.89	
2	$(R/S\text{-FO})_{0.1}–(PFNa)_{0.9}$	425	8.92	1.23	424	1.01	1.4	
		443		2.02	448		1.1	
3	$(R/S\text{-FO})_{0.1}–(PFPy)_{0.9}$	447	11.49	0.85	448	1.09	0.74	

values, macromolecule-based CP-OLEDs still exhibit significantly higher Q-factors than chiral small-molecular devices.

In addition to their superior $|g_{EL}|$ and Q-factor performance, CPL co-assembled macromolecular systems offer practical advantages such as mechanical flexibility and solution processability. These features make them especially attractive for further development of CP-OLED technologies.

6. Conclusions and outlooks

This review provides an overview of macromolecular co-assembly systems with intrinsic CPL properties reported since 2010. These systems can be categorized into three main types: (1) small-molecular chiral inducers–achiral luminescent macromolecules, (2) macromolecular chiral inducers–achiral luminescent small molecules, and (3) macromolecular chiral inducers–achiral luminescent macromolecules. From the perspective of macromolecular components, these studies encompass biomacromolecules such as DNA, peptides, and cellulose, as well as various synthetic polymers with repeating units. Through non-covalent interactions such as π–π stacking and electrostatic interactions, these macromolecules participate in co-assembly to form chiral supramolecular architectures with well-defined structures. Notably, these macromolecular chiral co-assemblies exhibit CPL with $|g_{lum}|$ values reaching magnitudes of 10^{-2} to 10^{-1}, significantly higher than traditional chiral luminescent small molecules, which typically exhibit $|g_{lum}|$ values in the range of 10^{-3} to 10^{-4}. Therefore, macromolecular co-assembly systems undoubtedly represent a promising alternative for achieving highly efficient CPL. Furthermore, compared to small molecules, macromolecules offer advantages such as greater molecular diversity and enhanced processability, making them more attractive for practical applications.

However, several challenges remain to be addressed in these macromolecular co-assembly systems. A primary concern is their CPL performance, particularly the $|g_{lum}|$, PLQY and EQE. While many macromolecular co-assembly systems introduced in this review have demonstrated $|g_{lum}|$ values reaching 10^{-2} to 10^{-1}, there remains a considerable gap compared to the theoretical maximum of 2 for a perfectly circularly polarized light source. This underscores the urgent need for new theoretical frameworks to elucidate the key factors governing $|g_{lum}|$ in co-assembly systems and to guide the rational design of macromolecular CPL materials with further enhanced dissymmetry factors. Additionally, improving the PLQY and electroluminescence EQE is equally critical for practical applications. Despite

recent efforts, the EQE of current CPL active macromolecular co-assemblies remains extremely low, often below 1%. Even with FRET strategies, the highest reported EQE is only 4.6%, which is still far from the application requirements. Therefore, innovative luminescent macromolecular designs and advanced assembly strategies are needed to enhance both the PLQY and EQE, ultimately improving the overall performance of CPL materials.

Macromolecules in CPL systems can be classified into bio-macromolecules and synthetic polymers. From a bio-macromolecule perspective, co-assemblies based on biological macromolecules hold great promise for biomedical applications. While DNA, peptides, and cellulose have already been explored in CPL co-assembly systems, their luminescence performance requires further optimization. Additionally, expanding the range of biomacromolecules used in CPL systems could provide more functional diversity and adaptability for specific applications.

From the perspective of synthetic polymers, the types of polymers employed in current CPL co-assembly systems include homopolymers, alternating copolymers, and random copolymers. However, block copolymers remain largely unexplored, despite their potential to introduce novel design strategies for CPL-active co-assemblies. This absence may be attributed to the stringent synthetic requirements of block copolymers, which necessitate well-defined molecular weight distributions (PDI = 1) typically achieved through living polymerization techniques. In contrast, most luminescent and chiral macromolecular polymers reported in the literature are synthesized via transition-metal-catalyzed coupling polymerization, which often follows the Flory distribution with PDI = 2, making block copolymer synthesis challenging. Thus, an interesting research direction would be the development of luminescent block copolymers using living polymerization techniques such as anionic polymerization of olefins, transition-metal catalyzed coordination polymerization of olefins, and atom transfer radical polymerization (ATRP). Alternatively, developing new living coupling polymerization strategies with PDI ≈ 1 could provide a feasible pathway for block copolymer synthesis in CPL applications.

Additionally, in terms of emission types, current CPL co-assembly macromolecular systems are predominantly based on fluorescence, with phosphorescence and TADF being relatively rare. Therefore, future research should also focus on the construction of macromolecular co-assembly systems that exhibit CP-TADF and CP phosphorescence, particularly those with room-temperature phosphorescence, high-temperature

phosphorescence, or long-persistent phosphorescence, which would broaden the scope of CPL applications across diverse technological and industrial fields.

Data availability

Data availability is not applicable to this review article as no new data were created or analyzed in this study.

Author contributions

C.-F. C. revised and supervised the manuscript. M.-J. J. wrote the manuscript. M. L. was contributed to the manuscript preparation. All authors revised and finalized the manuscript.

Conflicts of interest

There are no conflicts to declare.

Acknowledgements

References

1 F. Song, Z. Zhao, Z. Liu, J. W. Y. Lam and B. Z. Tang, Circularly polarized luminescence from AIEgens, *J. Mater. Chem. C*, 2020, **8**, 3284–3301.

2 D.-W. Zhang, M. Li and C.-F. Chen, Recent advances in circularly polarized electroluminescence based on organic light-emitting diodes, *Chem. Soc. Rev.*, 2020, **49**, 1331–1343.

3 H. G. Brittain, Excited-state optical activity, 1987-1995, *Chirality*, 1996, **8**, 357–363.

4 W.-L. Zhao, M. Li, H.-Y. Lu and C.-F. Chen, Advances in helicene derivatives with circularly polarized luminescence, *Chem. Commun.*, 2019, **55**, 13793–13803.

5 S.-P. Wan, H.-Y. Lu, M. Li and C.-F. Chen, Advances in circularly polarized luminescent materials based on axially chiral compounds, *J. Photochem. Photobiol., C*, 2022, **50**, 100500.

6 M. Li and C.-F. Chen, Advances in circularly polarized electroluminescence based on chiral TADF-active materials, *Org. Chem. Front.*, 2022, **9**, 6441–6452.

7 J.-M. Teng, D.-W. Zhang and C.-F. Chen, Recent progress in circularly polarized luminescence of [2.2]paracyclophane derivatives, *ChemPhotoChem*, 2022, **6**, e202100228.

8 X. Wang, X. Gao, H. Zhong, K. Yang, B. Zhao and J. Deng, Three-level chirality transfer and amplification in liquid crystal supramolecular assembly for achieving full-color and white circularly polarized luminescence, *Adv. Mater.*, 2025, **37**, 2412805.

9 H. Zhong, X. Gao, B. Zhao and J. Deng, "Matching rule" for generation, modulation and amplification of circularly polarized luminescence, *Acc. Chem. Res.*, 2024, **57**, 1188–1201.

10 X. Wang, B. Zhao and J. Deng, Liquid crystals doped with chiral fluorescent polymer: multi-color circularly polarized fluorescence and room-temperature phosphorescence with high dissymmetry factor and anti-counterfeiting application, *Adv. Mater.*, 2023, **35**, 2304405.

11 H. Zheng, W. Li, W. Li, X. Wang, Z. Tang, S. X.-A. Zhang and Y. Xu, Uncovering the circular polarization potential of chiral photonic cellulose films for photonic applications, *Adv. Mater.*, 2018, **30**, 1705948.

12 J. Han, J. You, X. Li, P. Duan and M. Liu, Full-color tunable circularly polarized luminescent nanoassemblies of achiral aiegens in confined chiral nanotubes, *Adv. Mater.*, 2017, **29**, 1606503.

13 B. A. San Jose, J. Yan and K. Akagi, Dynamic switching of the circularly polarized luminescence of disubstituted polyacetylene by selective transmission through a thermotropic chiral nematic liquid crystal, *Angew. Chem., Int. Ed.*, 2014, **53**, 10641–10644.

14 M. Li, H. Hu, B. Liu, X. Liu, Z.-G. Zheng, H. Tian and W.-H. Zhu, Light-reconfiguring inhomogeneous soft helical pitch with fatigue resistance and reversibility, *J. Am. Chem. Soc.*, 2022, **144**, 20773–20784.

15 J. Luo, Y. Li, H. Li, Q. Li and Y. Cheng, Ultrastrong circularly polarized luminescence triggered by the synergistic effect of chiral coassembly and selective reflective cholesteric liquid crystal film, *ACS Mater. Lett.*, 2024, **6**, 2957–2963.

16 Y. Li, Y. Chen, J. Luo, Y. Quan and Y. Cheng, Light-driven sign inversion of circularly polarized luminescence enabled by dichroism modulation in cholesteric liquid crystals, *Adv. Mater.*, 2024, **36**, 2312331.

17 M.-J. Ji, W.-L. Zhao, M. Li and C.-F. Chen, Circularly polarized luminescence with high dissymmetry factors for achiral organic molecules in solutions, *Nat. Commun.*, 2025, **16**, 2940.

18 J. R. Brandt, X. Wang, Y. Yang, A. J. Campbell and M. J. Fuchter, Circularly polarized phosphorescent electroluminescence with a high dissymmetry factor from PHOLEDs based on a platinahelicene, *J. Am. Chem. Soc.*, 2016, **138**, 9743–9746.

19 H. Maeda, Y. Bando, K. Shimomura, I. Yamada, M. Naito, K. Nobusawa, H. Tsumatori and T. Kawai, Chemical-stimuli-controllable circularly polarized luminescence from anion-responsive π-conjugated molecules, *J. Am. Chem. Soc.*, 2011, **133**, 9266–9269.

20 Q. Guo, M. Zhang, Z. Tong, S. Zhao, Y. Zhou, Y. Wang, S. Jin, J. Zhang, H.-B. Yao, M. Zhu and T. Zhuang, Multimodal-responsive circularly polarized luminescence security materials, *J. Am. Chem. Soc.*, 2023, **145**, 4246–4253.

21 P. Shen, S. Jiao, Z. Zhuang, X. Dong, S. Song, J. Li, B. Z. Tang and Z. Zhao, Switchable dual circularly polarized luminescence in through-space conjugated chiral foldamers, *Angew. Chem., Int. Ed.*, 2024, **63**, e202407605.

22 J. F. Sherson, H. Krauter, R. K. Olsson, B. Julsgaard, K. Hammerer, I. Cirac and E. S. Polzik, Quantum

teleportation between light and matter, *Nature*, 2006, **443**, 557–560.

23 Y. Imai, Y. Nakano, T. Kawai and J. Yuasa, A smart sensing method for object identification using circularly polarized luminescence from coordination-driven self-assembly, *Angew. Chem., Int. Ed.*, 2018, **57**, 8973–8978.

24 S. Shuvaev, M. A. Fox and D. Parker, Monitoring of the ADP/ATP ratio by induced circularly polarised europium luminescence, *Angew. Chem., Int. Ed.*, 2018, **57**, 7488–7492.

25 F. Furlan, J. M. Moreno-Naranjo, N. Gasparini, S. Feldmann, J. Wade and M. J. Fuchter, Chiral materials and mechanisms for circularly polarized light-emitting diodes, *Nat. Photonics*, 2024, **18**, 658–668.

26 K. Takaishi, T. Yamamoto, S. Hinoide and T. Ema, Helical oligonaphthodioxepins showing intense circularly polarized luminescence (CPL) in solution and in the solid state, *Chem.–Eur. J.*, 2017, **23**, 9249–9252.

27 Z. Jiang, T. Gao, H. Liu, M. S. S. Shaibani and Z. Liu, Easily accessible axial chiral binaphthalene-triarylborane dyes displaying intense circularly polarized luminescence both in solution and in solid-state, *Dyes Pigm.*, 2020, **175**, 108168.

28 Y. Sheng, D. Shen, W. Zhang, H. Zhang, C. Zhu and Y. Cheng, Reversal circularly polarized luminescence of AIE-active chiral binaphthyl molecules from solution to aggregation, *Chem.–Eur. J.*, 2015, **21**, 13196–13200.

29 M. Sawai, S. Matsumoto, Y. Mimura, Y. Imai, S. Yamazaki, N. Kanehisa, N. Tohnai, E. Nakata and H. Takashima, Circularly polarized luminescence (CPL) characteristics of hydrophobic pyrene derivatives/γ-cyclodextrin (γ-CD) complexes in aqueous solution dissolved by grinding, *J. Inclusion Phenom. Macrocyclic Chem.*, 2022, **102**, 133–142.

30 J. L. Lunkley, D. Shirotani, K. Yamanari, S. Kaizaki and G. Muller, Extraordinary circularly polarized luminescence activity exhibited by cesium tetrakis(3-heptafluoro-butyryl-(+)-camphorato) Eu(III) complexes in EtOH and CHCl₃ solutions, *J. Am. Chem. Soc.*, 2008, **130**, 13814–13815.

31 Y. B. Tan, Y. Okayasu, S. Katao, Y. Nishikawa, F. Asanoma, M. Yamada, J. Yuasa and T. Kawai, Visible circularly polarized luminescence of octanuclear circular Eu(III) helicate, *J. Am. Chem. Soc.*, 2020, **142**, 17653–17661.

32 M. Tsurui, R. Takizawa, Y. Kitagawa, M. Wang, M. Kobayashi, T. Taketsugu and Y. Hasegawa, Chiral tetrakis Eu(III) complexes with ammonium cations for improved circularly polarized luminescence, *Angew. Chem., Int. Ed.*, 2024, **63**, e202405584.

33 E. M. Sánchez-Carnerero, A. R. Agarrabeitia, F. Moreno, B. L. Maroto, G. Muller, M. J. Ortiz and S. de la Moya, Circularly polarized luminescence from simple organic molecules, *Chem.–Eur. J.*, 2015, **21**, 13488–13500.

34 J. Han, D. Yang, X. Jin, Y. Jiang, M. Liu and P. Duan, Enhanced circularly polarized luminescence in emissive charge-transfer complexes, *Angew. Chem., Int. Ed.*, 2019, **58**, 7013–7019.

35 J. Harris, V. Grillo, E. Mafakheri, G. C. Gazzadi, S. Frabboni, R. W. Boyd and E. Karimi, Structured quantum waves, *Nat. Phys.*, 2015, **11**, 629–634.

36 Z. Wang, M. Gao, S. Ren, X. Hao and W. Qin, Magnetic and electric control of circularly polarized emission through tuning chirality-generated orbital angular momentum in organic helical polymeric nanofibers, *Adv. Mater.*, 2019, **31**, 1904857.

37 K. Michaeli, N. Kantor-Uriel, R. Naaman and D. H. Waldeck, The electron's spin and molecular chirality – how are they related and how do they affect life processes?, *Chem. Soc. Rev.*, 2016, **45**, 6478–6487.

38 J. M. Abendroth, N. Nakatsuka, M. Ye, D. Kim, E. E. Fullerton, A. M. Andrews and P. S. Weiss, Analyzing spin selectivity in DNA-mediated charge transfer *via* fluorescence microscopy, *ACS Nano*, 2017, **11**, 7516–7526.

39 A. Kumar, E. Capua, M. K. Kesharwani, J. M. L. Martin, E. Sitbon, D. H. Waldeck and R. Naaman, Chirality-induced spin polarization places symmetry constraints on biomolecular interactions, *Proc. Natl. Acad. Sci. U. S. A.*, 2017, **114**, 2474–2478.

40 Y. Sang, J. Han, T. Zhao, P. Duan and M. Liu, Circularly polarized luminescence in nanoassemblies: generation, amplification, and application, *Adv. Mater.*, 2020, **32**, 1900110.

41 J. Kumar, T. Nakashima and T. Kawai, Circularly polarized luminescence in chiral molecules and supramolecular assemblies, *J. Phys. Chem. Lett.*, 2015, **6**, 3445–3452.

42 J. Roose, B. Z. Tang and K. S. Wong, Circularly-polarized luminescence (CPL) from chiral AIE molecules and macrostructures, *Small*, 2016, **12**, 6495–6512.

43 Z.-L. Gong, X. Zhu, Z. Zhou, S.-W. Zhang, D. Yang, B. Zhao, Y.-P. Zhang, J. Deng, Y. Cheng, Y.-X. Zheng, S.-Q. Zang, H. Kuang, P. Duan, M. Yuan, C.-F. Chen, Y. S. Zhao, Y.-W. Zhong, B. Z. Tang and M. Liu, Frontiers in circularly polarized luminescence: molecular design, self-assembly, nanomaterials, and applications, *Sci. China: Chem.*, 2021, **64**, 2060–2104.

44 B.-H. Liu, Y. Zong, N. Liu and Z.-Q. Wu, Advances in self-assembly-based circularly polarized luminescent materials, *Sci. China: Chem.*, 2024, **67**, 3247–3257.

45 Y. Deng, M. Wang, Y. Zhuang, S. Liu, W. Huang and Q. Zhao, Circularly polarized luminescence from organic micro-/nano-structures, *Light: Sci. Appl.*, 2021, **10**, 76.

46 D. Yang, P. Duan and M. Liu, Dual upconverted and downconverted circularly polarized luminescence in donor–acceptor assemblies, *Angew. Chem., Int. Ed.*, 2018, **57**, 9357–9361.

47 H. Zhang, J. Han, X. Jin and P. Duan, Improving the overall properties of circularly polarized luminescent materials through arene–perfluoroarene interactions, *Angew. Chem., Int. Ed.*, 2021, **60**, 4575–4580.

48 Q. Cheng, A. Hao and P. Xing, Eutectogels as matrices to manipulate supramolecular chirality and circularly polarized luminescence, *ACS Nano*, 2022, **16**, 6825–6834.

49 Y. Zhang, H. Li, Z. Geng, W. Zheng, Y. Quan and Y. Cheng, Dynamically stable and amplified circularly polarized excimer emission regulated by solvation of chiral co-assembly process, *Nat. Commun.*, 2022, **13**, 4905.

50 Z. Wang, A. Hao and P. Xing, Transpositional circularly polarized luminescence from transient charge-transfer coassembly, *Small*, 2021, **17**, 2104499.

51 F. Wang, W. Ji, P. Yang and C.-L. Feng, Inversion of circularly polarized luminescence of nanofibrous hydrogels through co-assembly with achiral coumarin derivatives, *ACS Nano*, 2019, **13**, 7281–7290.

52 K. Watanabe, H. Iida and K. Akagi, Circularly polarized blue luminescent spherulites consisting of hierarchically assembled ionic conjugated polymers with a helically π-stacked structure, *Adv. Mater.*, 2012, **24**, 6451–6456.

53 Y. Yang, R. C. da Costa, D.-M. Smilgies, A. J. Campbell and M. J. Fuchter, Induction of circularly polarized electroluminescence from an achiral light-emitting polymer *via* a chiral small-molecule dopant, *Adv. Mater.*, 2013, **25**, 2624–2628.

54 D.-M. Lee, J.-W. Song, Y.-J. Lee, C.-J. Yu and J.-H. Kim, Control of circularly polarized electroluminescence in induced twist structure of conjugate polymer, *Adv. Mater.*, 2017, **29**, 1700907.

55 K. Yao, Y. Shen, Y. Li, X. Li, Y. Quan and Y. Cheng, Ultrastrong red circularly polarized luminescence promoted from chiral transfer and intermolecular Förster resonance energy transfer in ternary chiral emissive nematic liquid crystals, *J. Phys. Chem. Lett.*, 2021, **12**, 598–603.

56 Y. Chen, Z. Xu, W. Hu, X. Li, Y. Cheng and Y. Quan, Strong-induced CPL emission promoted from achiral conjugated polymer-containing emissive nematic liquid crystals (P-N*-LCs), *Macromol. Rapid Commun.*, 2021, **42**, 2000548.

57 O. P. Lee, A. T. Yiu, P. M. Beaujuge, C. H. Woo, T. W. Holcombe, J. E. Millstone, J. D. Douglas, M. S. Chen and J. M. J. Fréchet, Efficient small molecule bulk heterojunction solar cells with high fill factors *via* pyrene-directed molecular self-assembly, *Adv. Mater.*, 2011, **23**, 5359–5363.

58 S. Hu, L. Hu, X. Zhu, Y. Wang and M. Liu, Chiral V-shaped pyrenes: hexagonal packing, superhelix, and amplified chiroptical performance, *Angew. Chem., Int. Ed.*, 2021, **60**, 19451–19457.

59 D. Niu, Y. Jiang, L. Ji, G. Ouyang and M. Liu, Self-assembly through coordination and π-stacking: controlled switching of circularly polarized luminescence, *Angew. Chem., Int. Ed.*, 2019, **58**, 5946–5950.

60 Z. Yang, Y. Wang, X. Liu, R. T. Vanderlinden, R. Ni, X. Li and P. J. Stang, Hierarchical self-assembly of a pyrene-based discrete organoplatinum(II) double-metallacycle with triflate anions *via* hydrogen bonding and its tunable fluorescence emission, *J. Am. Chem. Soc.*, 2020, **142**, 13689–13694.

61 Y. Zhang, H. Li, Z. Geng, W.-H. Zheng, Y. Quan and Y. Cheng, Inverted circularly polarized luminescence behavior induced by helical nanofibers through chiral co-assembly from achiral liquid crystal polymers and chiral inducers, *ACS Nano*, 2022, **16**, 3173–3181.

62 P. Zhao, W.-C. Guo, H.-Y. Lu and C.-F. Chen, High-performance white circularly polarized photoluminescence and electroluminescence from multi-emission enantiomers, *Angew. Chem., Int. Ed.*, 2025, **64**, e202424918.

63 P. Zhao, W.-C. Guo, M. Li, H.-Y. Lu and C.-F. Chen, Single-molecule white circularly polarized photoluminescence and electroluminescence from dual-emission enantiomers, *Angew. Chem., Int. Ed.*, 2024, **63**, e202409020.

64 Y. Zhang, Y. Li, Y. Quan, S. Ye and Y. Cheng, Remarkable white circularly polarized electroluminescence based on chiral co-assembled helix nanofiber emitters, *Angew. Chem., Int. Ed.*, 2023, **62**, e202214424.

65 K.-K. Tan, W.-C. Guo, W.-L. Zhao, M. Li and C.-F. Chen, Self-assembled chiral polymers exhibiting amplified circularly polarized electroluminescence, *Angew. Chem., Int. Ed.*, 2024, **63**, e202412283.

66 M. Bayat, H. Mardani, H. Roghani-Mamaqani and R. Hoogenboom, Self-indicating polymers: a pathway to intelligent materials, *Chem. Soc. Rev.*, 2024, **53**, 4045–4085.

67 W.-L. Zhao, W.-C. Guo, K. K. Tan, Z.-X. Yu, M. Li and C.-F. Chen, Chiral co-assembly based on a stimuli-responsive polymer towards amplified full-color circularly polarized luminescence, *Angew. Chem., Int. Ed.*, 2025, **64**, e202416863.

68 G. Zhang, Y. Bao, M. Pan, N. Wang, X. Cheng and W. Zhang, Memorable full-color circularly polarized luminescence from chiral co-assembled polymer films enabled by multipath transfer, *Sci. China: Chem.*, 2023, **66**, 1169–1178.

69 M. Pan, G. Zhang, H. Ma, X. Cheng, J. Li and W. Zhang, In situ thermoresponsive supramolecular assembly for switchable circularly polarized luminescence, *Sci. China: Chem.*, 2024, **67**, 2362–2372.

70 D. Liu, J. Zhao, X. Zhao, S. Shi, S. Li, Y. Wang, Q. Song, X. Cheng and W. Zhang, Chiral polymer micro/nano-objects: evolving preparation strategies in heterogeneous polymerization, *Sci. China: Chem.*, 2025, **68**, 1779–1793.

71 N. Wang, R. Hong, G. Zhang, M. Pan, Y. Bao and W. Zhang, Molecular imprinting strategy enables circularly polarized luminescence enhancement of recyclable chiral polymer films, *Small*, 2025, **21**, 2409078.

72 G. Zhang and W. Zhang, New concept on the generation and regulation of circularly polarized luminescence, *Chem.–Eur. J.*, 2025, **31**, e202404020.

73 X. Wang, Q. Song, Z. He, G. Zhang, T. Miao, X. Cheng and W. Zhang, Constructing diverse switchable circularly polarized luminescence *via* a single azobenzene polymer film, *Chin. Chem. Lett.*, 2025, **36**, 110047.

74 G. Zhang, X. Cheng, Y. Wang and W. Zhang, Supramolecular chiral polymeric aggregates: construction and applications, *Aggregate*, 2023, **4**, e262.

75 Y. Bao, G. Zhang, N. Wang, M. Pan and W. Zhang, Circularly polarized luminescent organogels based on fluorescence resonance energy transfer in an achiral polymer system, *J. Mater. Chem. C*, 2023, **11**, 2475–2479.

76 G. Zhang, Y. Bao, H. Ma, N. Wang, X. Cheng, Z. He, X. Wang, T. Miao and W. Zhang, Precise modulation of circularly polarized luminescence *via* polymer chiral co-assembly and contactless dynamic chiral communication, *Angew. Chem., Int. Ed.*, 2024, **63**, e202401077.

77 M. Hasegawa, W. Xiao, Y. Ishida, K. Asahi, H. Nishikawa, R. Ohno, D. Hayauchi, M. Hasegawa and Y. Mazaki, Synthesis and chiroptical properties of radially extended carbazole with chiral [2.2]paracyclophane core, *Adv. Funct. Mater.*, 2024, **34**, 2315215.

78 Y. Zhang, D. Li, Q. Li, Y. Quan and Y. Cheng, High comprehensive circularly polarized electroluminescence performance improved by chiral coassembled host materials, *Adv. Funct. Mater.*, 2023, **33**, 2309133.

79 W.-C. Guo, W.-L. Zhao, K.-K. Tan, M. Li and C.-F. Chen, B,N-embedded hetero[9]helicene toward highly efficient circularly polarized electroluminescence, *Angew. Chem., Int. Ed.*, 2024, **63**, e202401835.

80 C.-H. Guo, Y. Zhang, W.-L. Zhao, K.-K. Tan, L. Feng, L. Duan, C.-F. Chen and M. Li, Chiral co-assembly with narrowband multi-resonance characteristics for high-performance circularly polarized organic light-emitting diodes, *Adv. Mater.*, 2024, **36**, 2406550.

81 M. Górecki, F. Zinna, T. Biver and L. Di Bari, Induced circularly polarized luminescence for revealing DNA binding with fluorescent dyes, *J. Pharm. Biomed. Anal.*, 2017, **144**, 6–11.

82 Q. Jiang, X. Xu, P.-A. Yin, K. Ma, Y. Zhen, P. Duan, Q. Peng, W.-Q. Chen and B. Ding, Circularly polarized luminescence of achiral cyanine molecules assembled on DNA templates, *J. Am. Chem. Soc.*, 2019, **141**, 9490–9494.

83 X. J. Feng, P. L. Wu, F. Bolze, H. W. C. Leung, K. F. Li, N. K. Mak, D. W. J. Kwong, J.-F. Nicoud, K. W. Cheah and M. S. Wong, Cyanines as new fluorescent probes for DNA detection and two-photon excited bioimaging, *Org. Lett.*, 2010, **12**, 2194–2197.

84 M. Li, M. Liu and Y. Sha, Induced and inversed circularly polarized luminescence of achiral thioflavin T assembled on peptide fibril, *Small*, 2022, **18**, 2106130.

85 Z. Geng, Y. Zhang, Y. Zhang, Y. Quan and Y. Cheng, Amplified circularly polarized electroluminescence behavior triggered by helical nanofibers from chiral co-assembly polymers, *Angew. Chem., Int. Ed.*, 2022, **61**, e202202718.

86 X. Gao, J. Wang, K. Yang, B. Zhao and J. Deng, Regulating the helical chirality of racemic polyacetylene by chiral polylactide for realizing full-color and white circularly polarized luminescence, *Chem. Mater.*, 2022, **34**, 6116–6128.

87 H. Zhong, B. Zhao and J. Deng, Solvent-dependent chirality transmission and amplification from cellulose derivative to achiral helical polymer for achieving full-color and white circularly polarized luminescence, *Angew. Chem., Int. Ed.*, 2025, **64**, e202418463.

88 K. Yang, R. Zhang, Y. Liu, B. Zhao, Y. Wu and J. Deng, Circularly polarized phosphorescence energy transfer combined with chirality-selective absorption for modulating full-color and white circularly polarized long afterglow, *Angew. Chem., Int. Ed.*, 2024, **63**, e202409514.

89 S. Ma, H. Ma, K. Yang, Z. a. Tan, B. Zhao and J. Deng, Intense circularly polarized fluorescence and room-temperature phosphorescence in carbon dots/chiral helical polymer composite films, *ACS Nano*, 2023, **17**, 6912–6921.

90 D. Li, Z. Jiang, S. Zheng, C. Fu, P. Wang and Y. Cheng, Tunable circularly polarized electroluminescence behaviors from chiral co-assembled conjugated liquid crystal polymers, *J. Colloid Interface Sci.*, 2025, **678**, 1213–1222.